Molecular Crystals and Liquid Crystals Science and Technology. Section A. Molecular Crystals and Liquid Crystals

Publication details, including instructions for authors and subscription information:
http://www.tandfonline.com/loi/gmcl19

Dynamics of Giant Vesicles

Udo Seifert [a]

[a] Max-Planck-Institut für Kolloid- und Grenzflächenforschung, Kantstrasse 55, 14513, Teltow-Seehof, Germany

Version of record first published: 24 Sep 2006

To cite this article: Udo Seifert (1997): Dynamics of Giant Vesicles, Molecular Crystals and Liquid Crystals Science and Technology. Section A. Molecular Crystals and Liquid Crystals, 292:1, 213-225

To link to this article: http://dx.doi.org/10.1080/10587259708031932

Mol. Cryst. Liq. Cryst., 1997, Vol. 292, pp. 213–225
Reprints available directly from the publisher
Photocopying permitted by license only

Dynamics of Giant Vesicles

UDO SEIFERT*

Max-Planck-Institut für Kolloid- und Grenzflächenforschung, Kantstrasse 55, 14513 Teltow-Seehof, Germany

The dynamics of vesicle shape transformations are governed by the competition between curvature energy, geometrical constraints and viscous dissipation in the surrounding liquid. After a discussion of the general principles, three examples illustrate these concepts. (i) Slow conformal diffusion of vesicles of higher genus arises from the invariance of the curvature elasticity with respect to conformal transformations, (ii) spinodal fluctuations indicate the onset of the budding instability, and (iii) the dynamic pearling instability of cylindrical vesicles is caused by the action of laser tweezers.

Keywords: Membranes; dynamics; curvature energy; viscous damping; fluctuations; marginal stability criterion

1. INTRODUCTION

Giant vesicles of phospholipid membranes show an amazing variety of shapes among which transformations can be induced easily by varying external parameters such as temperature. The flexibility of the membrane arises from the fluidity of the lipid molecules within each monolayer which are in a smectic A state. Vesicles and their transformations can be observed and recorded by video microscopy [1].

Configurational changes of vesicles comprise two conceptually different aspects. First, thermal agitation generates dynamical equilibrium fluctuations around the shape of lowest energy. Since the typical time-scale for long wave-length fluctuations of micron-size vesicles is of the order of seconds, these fluctuations can be seen with video microscopy [2, 3]. Second, in any discontinuous shape transformation an unstable shape decays towards the new minimum by an essentially deterministic motion. In both cases, the presence of the surrounding liquid into which the membrane is embedded

*Tel: 49 3328 46594; Fax: 49 3328 46212; E-mail: Useifert@mpikg-teltow.mpg.de

determines the dynamics in an important non-trivial way, since it generates an effective long-range dynamical interaction along the membrane.

In this article, I will describe in non-technical terms recent work on dynamics of vesicles using three example. These examples are chosen because they illustrate nicely how progress in this field arises from fruitful interaction between theory and experiment. In Sect. II, the basic physical concepts of the curvature model for vesicles and the dynamics of membranes are recalled. Sect. III deals with the slow conformal diffusion of vesicle shapes of higher topology. This phenomenon was first predicted [4] to arise from an invariance of the curvature energy and then observed experimentally [5]. Sect. IV. gives an example of growing fluctuations as a mechanical instability of a vesicle shape is approached [6]. In Sect. V, the pearling instability of cylindrical vesicles induced by the action of laser tweezers will be described [7–9].

2. BASIC PRINCIPLES

A. Curvature Elasticity

The equilibrium shapes of vesicles arise from a competition between the bending elasticity of the membrane and geometrical constraints such as a fixed surface area, A, and fixed enclosed volume, V. Because of the length-scale separation between the thickness of the bilayer ($\sim 4\,\mathrm{nm}$) and the diameter of a vesicle ($\sim 1-40\,\mu\mathrm{m}$), the membrane can be described as a two-dimensional surface embedded in three-dimensional space. Such a surface is locally characterized by the mean curvature H and the Gaussian curvature K. Since the integral over the latter is a topological invariant, only H contributes non-trivially to the bending energy [10–13]

$$W \equiv F_1 + F_2 \equiv \frac{\kappa}{2}\oint (2H)^2\, dA + \frac{\alpha\pi\kappa}{8Ad^2}(\Delta A - \Delta A_0)^2. \tag{1}$$

The energy scale is set by the bending rigidity κ. The second term arises from the fact that lipid molecules do not flip substantially between the two monolayers during the time-scale (minutes to hours) of a typical experiment. Therefore, the area difference $\Delta A = 4d \oint H dA$ between the neutral planes of the two monolayers, which are a distance $2d$ apart, has an optimal value $\Delta A_0 \equiv (N^+ - N^-)/\phi_0$ dependent on the number difference of molecules in the two layers and their equilibrium density ϕ_0. Any deviation of such a

match costs an energy which is comparable to the first term since the material parameter α is of order unity [13].

The geometrical constraints of controlled surface area and controlled enclosed volume arise from the insolubility of the lipid molecules and the unavoidable presence of osmotically active molecules in the enclosed volume, respectively. Minimization of W at fixed area and volume yields a variety of shapes, such as prolate and oblate ellipsoids, pears, and shapes of non-spherical topology [1].

B. Hydrodynamics

Knowledge of the energy of any vesicle configuration is a necessary but not sufficient condition in order to formulate a theory of dynamic shape transformations. To do so, one also needs equations of motion [14–17]. Because the crucial dissipation in these process arises in the embedding liquid, one has to start from the Navier Stokes equations for this liquid. Since for typical phenomena the motion is always overdamped, the inertial terms can be neglected. Thus, one arrives at the force balance for the velocity field $\mathbf{v}(\mathbf{r})$ of the solvent with viscosity η

$$\nabla p - \eta \nabla^2 v = \mathbf{K}(\mathbf{r}). \tag{2}$$

Here, $p(\mathbf{r})$ denotes the pressure, and $\mathbf{K}(\mathbf{r})$ are the external forces acting on the liquid. These include both forces exerted from the membrane and forces due to confining boundaries, such as the presence of a substrate in the case of adhesion. For these phenomena, the liquid can be considered as incompressible, $\nabla \cdot \mathbf{v} = 0$, which can be used to eliminate the pressure in (2) in favor of the forces.

The formal solution to this equation gives the velocity at any point in real space as a function of the external forces

$$\mathbf{v}(\mathbf{r}) = \int d^3 r' \, \mathcal{O}(\mathbf{r}, \mathbf{r}') \, \mathbf{K}(\mathbf{r}'), \tag{3}$$

where the Oseen tensor $\mathcal{O}(\mathbf{r}, \mathbf{r}')$, in Cartesian co-ordinates, has matrix elements [18]

$$O_{ij}(\mathbf{r}, \mathbf{r}') \equiv \frac{1}{8\pi\eta |\mathbf{r} - \mathbf{r}'|} \left[\delta_{ij} + \frac{(r_i - r_i')(r_j - r_j')}{|\mathbf{r} - \mathbf{r}'|^2} \right]. \tag{4}$$

Thus, the hydrodynamics generates a long-range interaction ($\sim 1/|\mathbf{r} - \mathbf{r}'|$) through the velocity field.

Since essentially no liquid penetrates the membrane, the normal velocity of the liquid, $\mathbf{v}(\mathbf{R}(s_1, s_2)) \cdot \mathbf{n}(s_1, s_2)$, at any point $\mathbf{R}(s_1, s_2)$ of the membrane can be identified with a configurational change of the membrane. Thus, we obtain a dynamical equation of motion for the membrane as

$$\partial_t \mathbf{R}(s_1, s_2, t) \cdot \mathbf{n}(s_1, s_2, t) = \mathbf{n}(s_1, s_2, t) \cdot \int d^3 r' \mathcal{O}(\mathbf{r}, \mathbf{r}') \mathbf{K}(\mathbf{r}'). \tag{5}$$

The crucial quantity here is the force density $\mathbf{K}(\mathbf{r})$ exerted by the membrane (and container walls in confined geometries) upon the liquid. In general, this force density has normal and tangential components. Both curvature energy and tension contributes to the normal component while the tangential components are dominated by forces within the membrane such as lateral tension gradients. Such an inhomogeneous tension can arise from the local incompressibility of the membrane. For a compressible membrane, the density has its own equation of motions. If the membrane is modeled as a bilayer, viscous friction between the two monolayers has also to be taken into account [16]. The tangential forces have to be determined self-consistently from the no-slip boundary conditions between the membrane and the embedding liquid.

For an arbitrary membrane configuration, geometry complicates the problem even further. A fluid membrane has to obey reparametrization invariance. Stochastic forces have to be introduced to describe the thermal fluctuations. The correlator of these forces has to be properly chosen to ensure that such a dynamics produces the correct equilibrium. A general formulation of membrane hydrodynamics which takes care of all these subtleties has recently been given in Ref. [17]. So far, such a general formulation has not been successfully transformed into numerically stable algorithms due to the complexity of the problem. Progress has been achieved mainly by two routes. One can either truncate all the complexity and focus on what scaling and symmetry arguments dictate. Two examples of such an approach are discussed below. Alternatively, one can expand the dynamics around simple equilibrium conformations, such as a free or a bound membrane [19]. A less trivial case of the latter approach is the pearling instability discussed in Sect. V.

C. Almost Planar Membrane

It is instructive to discuss briefly the dispersion relation of an almost planar bilayer parametrized by a local height field $h(x, y)$ in a Monge representa-

tion [14,16]. Keeping only quadratic terms in an expansion of the curvature energy around a flat membrane, each Fourier mode with wave-vector $\mathbf{q}$ carries an energy $E_0(q) \equiv \kappa q^4$. Assuming an incompressible membrane and no-slip boundary conditions between membrane and surrounding liquid leads to the equation of motion for the Fourier amplitude h_q.

$$\partial_t h_{\mathbf{q}} = -\Gamma_0(q) E_0(q) h_{\mathbf{q}}. \tag{6}$$

The "kinetic coefficient"

$$\Gamma_0(q) = 1/4\eta q \tag{7}$$

reflects the long range character of the hydrodynamic damping. In the solution to this equation of motion,

$$h_{\mathbf{q}}(t) = h_{\mathbf{q}}(0) e^{-\gamma_0(q)t}, \tag{8}$$

the damping rate $\gamma_0(q)$ is easily identified as

$$\gamma_0(q) = \Gamma_0(q) E_0(q) = \kappa q^3/4\eta. \tag{9}$$

The form (9) of the damping rate as a product [20] of a kinetic coefficient which contains the dissipation, and an energy which contains the driving force, is characteristic of the low Reynolds number viscous dynamics. Even though the numerical prefactors depend on the specific geometry, the scaling embodied in (9) can also be applied to bending fluctuation of quasi-spherical vesicles [15]. Thus, the slowest modes of these shapes have the characteristic relaxation rate $\kappa/\eta R^3$.

3. CONFORMAL DIFFUSION

For vesicles with at least two holes or handles, the shape of minimal energy is not unique in a large part of the phase diagram. This degeneracy arises from the conformal invariance of the first term, F_1, in the energy (1) [4].

Thus, the local curvature energy F_1 does not change if a vesicle shape is subject to a conformal transformation. The non-trivial conformal transformations are inversions in a unit sphere centered at an arbitrary point $\mathbf{R}_s$

$$\mathbf{R} \rightarrow \mathbf{R}_s + (\mathbf{R} - \mathbf{R}_s)/(\mathbf{R} - \mathbf{R}_s)^2 \tag{10}$$

For many applications it is more convenient to use a special conformal transformation, which consist of an inversion in a unit sphere in the center, a translation along the vector $\mathbf{a}$ and another inversion in the same unit sphere. Because $\mathbf{a}$ is a three dimensional vector, the ground state energy F_1 for given topology is, in general, three-fold continuously degenerate. The constraint of a fixed area A can always be restored by a rescaling of the shape. The two constraints on the volume and the optimal area difference remove two directions of this degeneracy. Thus, for physical vesicles of genus 2 or higher, the shape of lowest energy is still one-fold continuously degenerate. Figure 1 shows an example of three theoretical shapes which have the same total curvature energy W and which obey the same geometrical constraints [4].

This degeneracy is predicted to have an observable effect: Thermal excitations will cause the shape of such a vesicle to change permanently via a diffusion process along the conformal trajectory. Experimentally, conformal diffusion has just recently been observed. Michalet and Bensimon [5] were able to find shapes which correspond to the theoretical shapes shown in Figure 1.

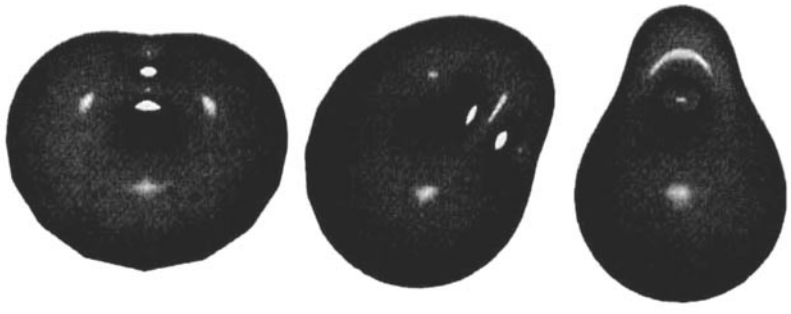

FIGURE 1 Three different genus-2 vesicles related by a conformal diffusion process. All shapes have the same area, the same enclosed volume, and the same area-difference between the two layers.

The dynamics of this diffusion process can be estimated by a simple scaling argument [4]. The typical time-scale t_{cf} for a significant shape change along the conformal trajectory is $t_{cf} = \eta R_0^3/T$. Note that this time-scale is a factor of $k/T \simeq 10$ slower than the time-scale for the long wavelength bending modes discussed above. Using the typical values $\eta = 10^{-2}$erg/cm^3, $R_0 = 10\,\mu$m, and $T = 4 \times 10^{-14}$erg, one finds a time scale of a few minutes which indeed corresponds to the experimental findings. The same estimate of the time-scale also holds for rotational diffusion.

4. SPINODAL FLUCTUATIONS

Whilst conformal diffusion is an example of a shape transformation that happens even for constant external parameters, most shape transformations associated with a change in energy require that some external parameter be altered. The paradigmatic example of such a shape change is the budding transition [1,21]. In this transition, an originally prolate shape becomes unstable with respect to a symmetry breaking pear mode as the temperature T increases. Before the instability actually sets in at $T = T_b$, pronounced fluctuations towards a pear shape build up and decay again [6]. Figure 2 shows a time sequence of snap shots of the contour of a prolate vesicle at fixed temperature close to the transition.

A complete modeling of the dynamics of the prolate shape with its fluctuations is prohibitively complex at present, but, fortunately, a simple theoretical picture suffices to describe the basic effect [6]. For such a description, the whole dynamics is projected onto a single mode with an "order parameter", i.e., an amplitude a. Symmetry of the prolate shape then dictates the following effective energy for the amplitude a of the pear mode [6]

$$W(a) = k[ra^2/2 - ga^4/4 + ua^6/6], \tag{11}$$

where the parameters, r, $g > 0$, and $u > 0$, are dimension-less. The symmetrical (prolate) branch loses metastability as $(T_b - T) \sim r \to 0^+$. Amplitude fluctuations are given at the Gaussian level by $\langle a^2 \rangle = k_B T/kr$, which is only expected to be valid when $\langle a^2 \rangle \ll r/g$, so the non-Gaussian terms may be neglected. Indeed, when this criterion is not satisfied, there is a significant probability of escape over the barrier. It follows that there is a range of temperature near, but not too near, the budding instability, for which the static fluctuations are predicted to grow as $(T_b - T)^{-1}$. Such a dramatic increase in the amplitude of pear-like fluctuations has indeed been observed experimentally [6].

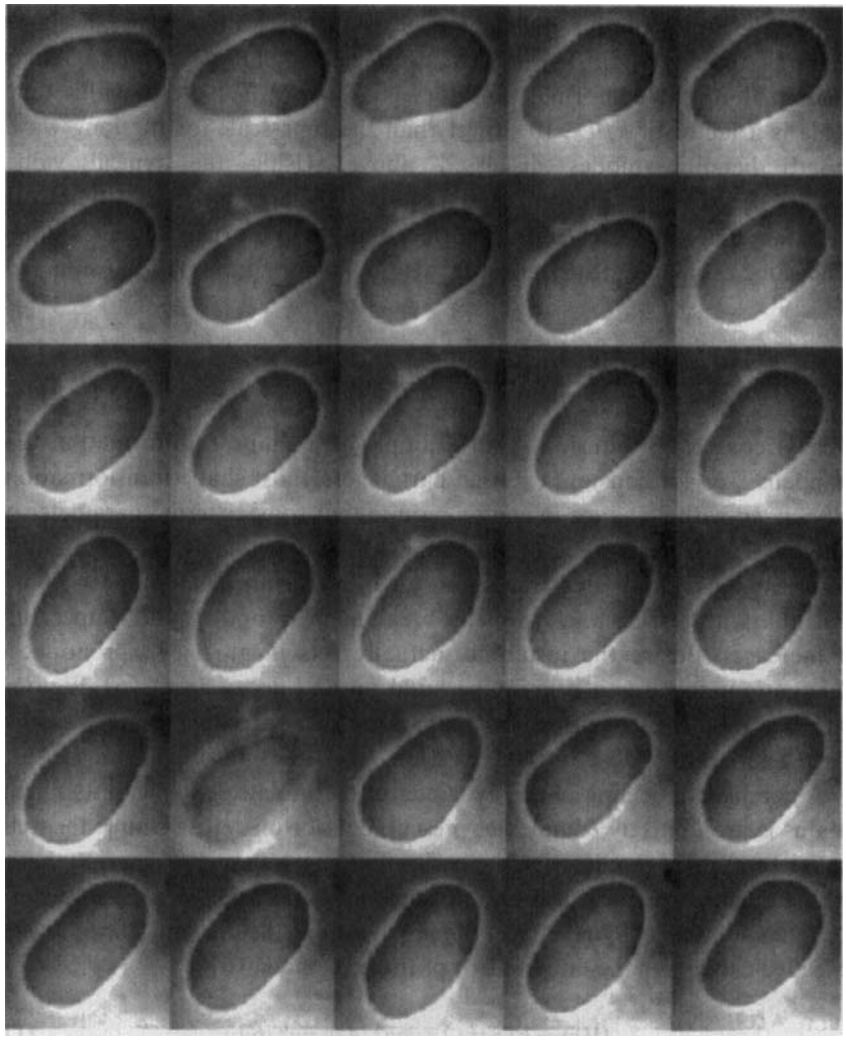

FIGURE 2 Snapshots of contours of a prolate vesicle at constant temperature. The time difference between each frame is 6.3 sec. Two slow, consecutive pear fluctuations are clearly visible. Courtesy of H.-G. Döbereiner.

The time dependence of the amplitude a requires a dynamical theory. In the one-mode picture the soft mode should obey a dynamical equation similar to the equation of motion of the planar membrane (6) [6],

$$\partial a/\partial t = -\Gamma \partial W/\partial a + \zeta, \tag{12}$$

where we make the usual noise term ζ explicit. Eq. (12) simplifies to $\partial a/\partial t = -\Gamma kra + \zeta$ near $a = 0$, when the Gaussian term dominates. The kinetic coefficient $\Gamma = c/\eta R^3$ contains as the appropriate length scale for the unstable mode the scale $R \simeq 10\,\mu m$ of the vesicle. The numerical factor c is of order unity. In the Gaussian regime Eq. (12) predicts

$$\langle a(t)a(0)\rangle = \langle a^2\rangle e^{-t/\tau}, \tag{13}$$

with $\tau = 1/(\Gamma kr) \sim 1/(T_b - T)$. Such an increase of the correlation time with temperature is indeed consistent with the observations [6].

While the onset of the budding instability can thus be quantitatively understood, little can be said about the dynamics of the decay of the prolate towards the new pear shaped minimum. Even though the deterministic dynamics of an axisymmetric contour, including the hydrodynamics of the surrounding liquid, can be formulated, the numerical solution of these equations is still plagued with spurious instabilities [22].

5. PEARLING INSTABILITY

Despite its very recent discovery [7], the laser-induced pearling instability of cylindrical vesicles is by now arguably the best-studied case of a dynamical shape transformation. Initial preparation of the system yields stable, nearly straight single bilayer cylinders up to hundreds of microns long, anchored at both ends by large globules of lipid. The tubules are polydisperse, with initial radii R_0 between 0.3–5 μm. Initially the system is somewhat flaccid, as seen from visible thermal undulations and the fact that the tubes are not quite straight.

Application of a laser spot localized to $\sim 0.3\mu m$ on such a cylindrical vesicle produces a dramatic transformation to a stationary "peristaltic" figure, i.e., a cylindrical shape whose radius at first varies roughly sinusoidally with distance z from the trap, see Figure 3. There is no evidence for any initial time delay between laser illumination and the onset of the instability. Greater laser power is required for larger-radius tubules, but nothing seems to depend on the length of the tube, so long as the trap is initially many radii from the ends. The shape transformation propagates outward from the laser trap, with a well-defined velocity v_f typically about $30\,\mu m/sec$. Remarkably, after a very short illumination the shape transformation continues to propagate after the laser is shut ofl, leading to a uniform, small-amplitude peristaltic shape. Longer excitation leads to a pearled state.

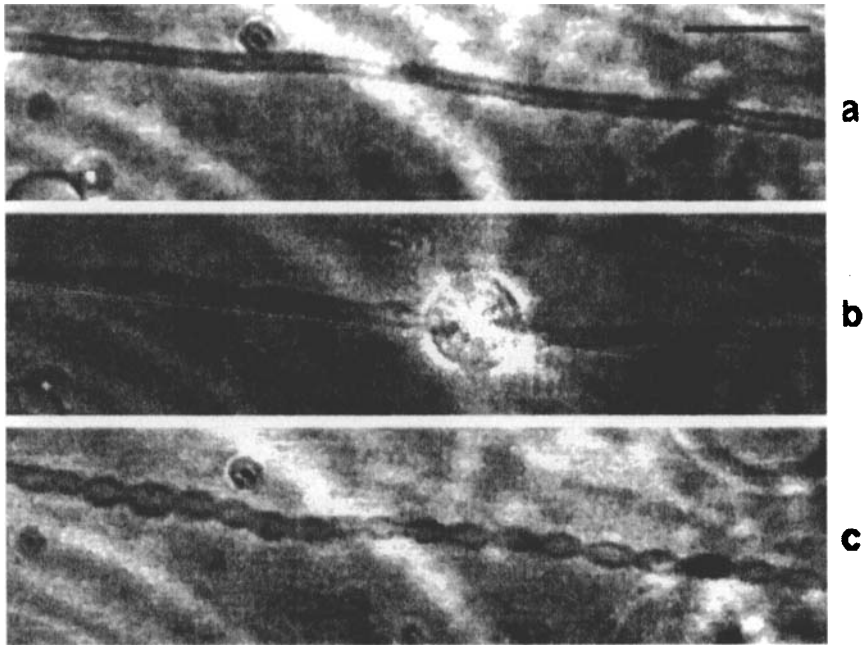

FIGURE 3 Laser-induced pearling instability of cylindrical vesicles. (a) Section of DMPC tube. (b) Initial instability upon tweezing marked by the circular reflection. State (c) eventually decays back to state (a) if laser is shut off. The bar denotes 10 μm. Courtesy of R. Bar-Ziv and E. Moses.

Once formed, the peristaltic shape has a well-defined initial wavelength which is uniform over many microns. Whatever the initial radius R_0 this wavelength is found to be $\lambda = 2\pi R_0/k_0$ where the dimension-less initial wavenumber k_0 is always in the range 0.64–1.0, and typically about 0.8. As the modulation grows more pronounced, k grows from k_0 to become slightly greater than 1, and deviations from a simple sinusoidal profile become pronounced. The modulated state is under tension: visible thermal fluctuations are suppressed and the tube draws itself straighter than initially.

The theoretical modeling [7–9,23] exploits the phenomenological resemblance with the classical Plateau-Rayleigh instability of cylindrical fluid jets subject to surface tension. For a volume preserving deformation of a cylinder under tension, the area decreases for any axisymmetric deformation with a wave number $k_0 < 1$. Therefore, a cylindrical shape under tension is unstable. In the presence of bending rigidity k, one needs a finite tension $\sum \geq 3k/2R_0^2$ to initiate this static instability [8].

The laser creates a local lateral tension of the order of 10^{-3}erg/cm^2 by sucking lipid into the trap [8,9]. This tension spreads rapidly along the cylinder since the membrane is nearly incompressible. After this very brief initial period, the cylinder is unstable towards all deformations with a wave number smaller than 1 just as in Rayleigh's case. The wave-length selection, however, depends crucially on the dynamics and, in particular, the boundary conditions at the cylinder. In the pearling instability, a material object, the bilayer membrane, separates the interior from the exterior fluid. Solving the corresponding hydrodynamical equations in the over-damped case along the lines discussed above for the planar geometry, one finds an equation of motion of the type (6) for small displacements around the homogeneous cylinder [8]. The growth rate $-\Gamma(q)E(q) > 0$ peaks at a wave vector $q_0 = 0.65/R_0$. Even though this value depends somewhat on the bending rigidity and the bilayer dynamics, it is mostly determined by the balance between the tension and the dissipation in the interior water for realistic parameters. Since the experiment shows the instability to propagate from the center, the fastest growing mode is not the best candidate for the actual pattern.

The propagating character of the instability is captured by using the concept of marginal stability [24,25]. This criterion, which applies to many propagating instabilities, is a theory of how an unstable state (here the plain cylinder after spread of the tension) starting from a localized excitation (here the laser spot) decays into a new stable minimum (here the pearled state) via front propagation. Since the marginal stability criterion requires only knowledge of the linearized dynamics around the unstable state, it can be worked out completely for the pearling instability. In fact, it leads to a much better value for the wave-number of the pattern of $q_0 \simeq 0.8/R_0$ in presumably somewhat fortuitous agreement with the experiment. Since it is a general short-coming of the marginal stability criterion that it cannot prove front propagation but rather assumes it, the analysis of [9] is backed up with a numerical solution of the full non-linear elastic energy using a lubrication approximation for the hydrodynamics. The numerical results, indeed, also show front propagation with roughly the same values as derived from the marginal stability criterion. The late stage dynamics, where the pearls move along the tether, is not yet understood. It could be caused by lateral gradients of tension.

6. CONCLUSION

The three examples of shape transformations described in this article illustrate the broad range of dynamical phenomena associated with vesicle

shape transformations. A manageable theory of dynamics of non trivial shapes is still lacking not because of ignorance of the basic equations but rather because of tremendous numerical problems modeling the fluid dynamics of an evolving three dimensional shape. Success has been achieved by focusing on simpler geometries, such as the onset of instability in the case of pearling, or by using an effective one mode-description as in the case of the spinodal fluctuations. Both conformal diffusion and spinodal fluctuations are stochastic phenomena for which not much more remains to be done on this level. However, the deterministic dynamics of both the decaying pear in the budding process and the late stage dynamics of the pearling instability will remain a challenge to the theory as long as the deterministic hydrodynamic equations cannot be solved numerically.

Acknowledgement

The work reported in this paper has been obtained in collaboration with numerous co-workers. I am grateful to all of them for many stimulating discussions and enjoyable interactions. I thank J. Shillcock for a critical reading of the manuscript.

References

[1] U. Seifert and R. Lipowsky, in *Structure and dynamics of membranes*, Vol. 1 of *Handbook of biological physics*, edited by R. Lipowsky and E. Sackmann (Elsevier, Amsterdam, 1995), pp. 403–64.
[2] H. Engelhardt, H. P. Duwe and E. Sackmann, *J. Physique Lett.*, **46**, L 395 (1985).
[3] I. Bivas, *et al.*, *J. Phys.*, **48**, 855 (1987).
[4] F. Jülicher, U. Seifert and R. Lipowsky, *Phys. Rev. Lett.*, **71**, 452 (1993).
[5] X. Michalet and D. Bensimon, *Science* **269**, 666 (1995).
[6] H.-G. Döbereiner, E. Evans, U. Seifert and M. Wortis, *Phys. Rev. Lett.*, **75**, 3360 (1995).
[7] R. Bar-Ziv and E. Moses, *Phys. Rev. Lett.*, **73**, 1392 (1994).
[8] P. Nelson, T. Powers and U. Seifert, *Phys. Rev. Lett.*, **74**, 3384 (1995).
[9] R. E. Goldstein, P. Nelson, T. Powers and U. Seifert, submitted to *J. Phys. II* (France) **6**, 767 (1996).
[10] P. B. Canham, *J. Theoret. Biol.*, **26**, 61 (1970).
[11] W. Helfrich, Z. Naturforsch, **28c**, 693 (1973).
[12] E. Evans, *Biophys. J.*, **14**, 923 (1974).
[13] L. Miao, U. Seifert, M. Wortis and H.-G. Döbereiner, *Phys. Rev.*, *E* **49**, 5389 (1994).
[14] F. Brochard and J. F. Lennon, *J. Physique* **36**, 1035 (1975).
[15] S. T. Milner and S. A. Safran, *Phys. Rev.*, *A* **36**, 4371 (1987).
[16] U. Seifert and S. A. Langer, *Europhys. Lett.*, **23**, 71 (1993).
[17] W. Cai and T. C. Lubensky, *Phys. Rev.*, *E* **52**, 4251 (1995).
[18] M. Doi and S. F. Edwards, *The Theory of polymer dynamics* (Clarendon Press, Oxford (1986).

[19] M. Kraus and U. Seifert, *J. Phys., II France* **4**, 1117 (1994).
[20] Y. Marathe and S. Ramaswamy, *Europhys. Lett.*, **8**, 581 (1989).
[21] J. Käs and E. Sackmann, *Biophys., J.* **60**, 825 (1991).
[22] S. A. Langer, private communication.
[23] R. Granek and Z. Olami, *J. Phys., II France* **5**, 1349 (1995).
[24] G. Dee and J. Langer, *Phys. Rev. Lett.*, **50**, 383 (1983).
[25] W. van Saarloos, *Phys. Rev., A* **37**, 211 (1988).